Ole Sigmund

Manufacturing tolerant topology optimization

Abstract In this paper we present an extension of the topology optimization method to include uncertainties during the fabrication of macro, micro and nano structures. More specifically, we consider devices that are manufactured using processes which may result in (uniformly) too thin (eroded) or too thick (dilated) structures compared to the intended topology. Examples are MEMS devices manufactured using etching processes, nano-devices manufactured using e-beam lithography or laser micro-machining and macro structures manufactured using milling processes. In the suggested robust topology optimization approach, under- and over-etching is modelled by image processing-based "erode" and "dilate" operators and the optimization problem is formulated as a worst case design problem. Applications of the method to the design of macro structures for minimum compliance and micro compliant mechanisms show that the method provides manufacturing tolerant designs with little decrease in performance. As a positive side effect the robust design formulation also eliminates the longstanding problem of one-node connected hinges in compliant mechanism design using topology optimization.

Keywords Topology optimization, Robust design, Compliant Mechanisms, Manufacturing constraints

1 Introduction

Macro, micro and nano structures fabricated using milling, etching or e-beam lithography processes are all vulnerable to manufacturing uncertainties. Carefully designed and optimized structures may have their performance degraded or even lose their functionality due to wear of machining tools, under- or over-etching, or malcalibrated e-beam equipment.

Figure 1 shows an example of a nano-photonic crystal based waveguide manufactured using a defocussed e-beam

Department of Mechanical Engineering, Solid Mechanics
Technical University of Denmark
Niels Koppel's Allé, Building 404, DK-2800 Lyngby, Denmark
Tel.: +45-45254256, Fax: +45-45931975
E-mail: sigmund@mek.dtu.dk

lithography equipment. The topology optimized waveguide [1] is shown at the top and the manufactured device is shown at the bottom[1]. It is clearly seen that all holes have become too big due to the badly focussed e-beam and that many small features have merged together in the physical structure. This error rendered the device useless and its waveguiding abilities have never been tested.

Another example that demonstrates the need for manufacturing robust optimal topologies is shown in Figure 2a. The bitmap picture shows a topology optimized compliant inverter mechanism [3,4]) (the exact formulation of the underlying design problem is defined in the Appendix). The problematic, so-called "one-node connected hinges" are clearly seen. These hinges are artificially stiff due to erroneous finite element modelling [3,5], they are related to the so-called checkerboard problem in topology optimization [6–8] and despite many attempts, no researchers have so far managed to get rid of them in systematic, mesh-independent and efficient ways (see e.g. refs. [5,9–12]). Filter techniques intended for removal of checkerboard instabilities are only partly successful in preventing the one-node connected hinges [3,13–16] although a very recently published level-set based scheme shows some promise [17] in this respect. Therefore in practice, the hinges are usually converted to slender compliant hinges in a manual post-processing process [18]. Apart from constituting erroneous finite element modelling and likely failure of a realized device, the narrow hinges are also very vulnerable to manufacturing uncertainties. In the underetched (dilated) mechanism in Figure 2b, the thin hinges have become thick and non-compliant and in the over-etched (eroded) mechanism in Figure 2c, the mechanism has become disconnected and useless.

Based on above examples, it is clear that robustness towards manufacturing uncertainties is highly desirable to be included in the topology optimization process a priori.

---

[1] Note that this particular example of a photonic crystal based waveguide device has no practical physical use. It was designed and manufactured for a celebration of professor Pauli Pedersen's (PP) in connection with his retirement at the 10th internal DCAMM Symposium (Danish Center for Applied Mathematics and Mechanics), April 2005.
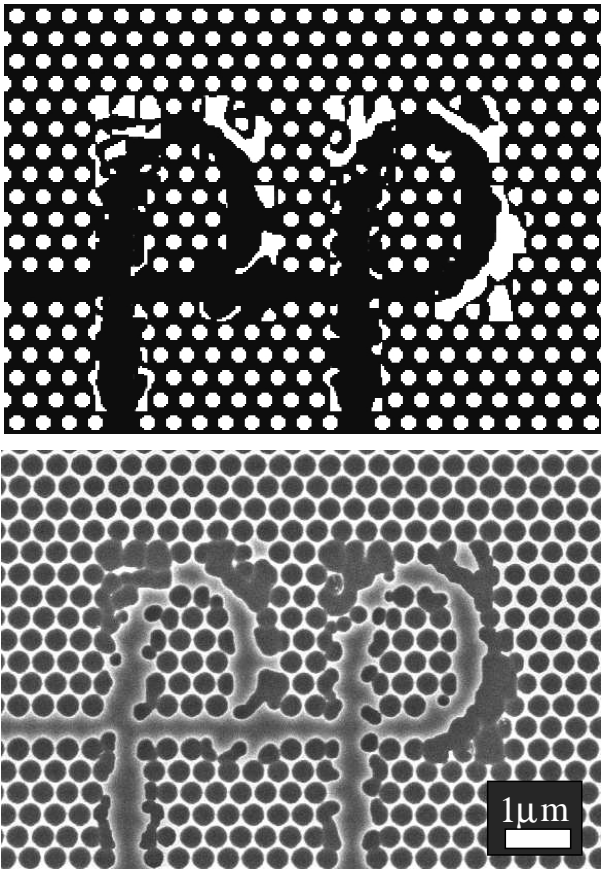
Fig. 1 Example of manufacturing failure due to unfocussed e-beam lithography process. Top: Topology optimized design of a photonic crystal based photonic waveguide splitter (c.f. [2]). Bottom: Waveguide manufactured using de-focussed e-beam lithography process where all holes are too large and fine details have disappeared.

a) Original topology
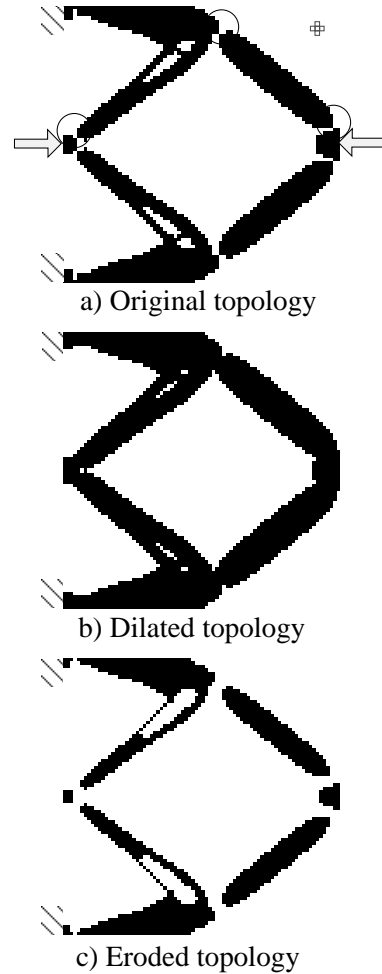
b) Dilated topology

c) Eroded topology

Fig. 2 Example of the morphology operators used on an optimized compliant mechanism image. a) Optimized density distribution. The circles indicate critical one-node connected hinges. b) "dilated" topology and c)"eroded" topology. The 5 element structuring element is also indicated.

Reliability-based and robust design methods have been developed for topology optimization in several works (see e.g. refs. [19–27]). For truss structures, uncertainties of nodal positions [28,29] as well as failure of individual bars [28] have been considered, but otherwise, uncertain properties have so far been limited to global variables like load magnitude and direction, overall dimensions and material properties, most probably due to the heavy computational cost associated with the inclusion of even a few non-deterministic design variables. To the author's best knowledge, nobody has so far attempted to include geometrical (density distribution) features like etching uncertainties as described above in robust or reliability-based continuum type topology optimization approaches.

Morphology-based image operators as means for feature size control in topology optimization were recently proposed by the author [16]. Here, it is suggested to formulate a deterministic design formulation that makes use of the morphology operators "erode" and "dilate" to model under- and/or over-etching of fabricated structures. The "dilate" filter is implemented by a Heaviside function approach suggested in

ref. [15] and the "erode" filter is implemented by a modified Heaviside function as suggested in ref. [16]. During the optimization process we work with the original density distribution as well as an eroded and/or a dilated density distribution. The goal of the optimization problem is to optimize the objective function for the worst case of these density distributions. In this way, we make sure that the optimized structure performs well for a correctly etched structure but also for an over-etched and/or an under-etched structure. By adjusting the filter size (i.e. the over- and under-etching depths), more or less manufacturing sensitive structures can be obtained.

The paper is organized as follows. The robust topology optimization problem formulation is given in Section 2, image morphology-based filtering techniques are discussed in Section 3, sensitivity analysis and numerical implementation are given in Section 4 and numerical examples are demon-

strated in Section 5. Section 6 summarizes the paper and exact formulations of the test cases are given in the Appendix.

2 Robust topology optimization formulation

In the density approach to topology optimization (see e.g. ref. [30]) the material distribution is described by the density distribution vector $\boldsymbol{\rho}$ (size equal to the number of finite elements). Here, we add an eroded density distribution vector denoted $\boldsymbol{\rho}^e = \boldsymbol{\rho}^e(\boldsymbol{\rho})$ and a dilated density distribution vector $\boldsymbol{\rho}^d = \boldsymbol{\rho}^d(\boldsymbol{\rho})$. Section 3 will discuss how $\boldsymbol{\rho}^e$ and $\boldsymbol{\rho}^d$ are computed from the original density distribution $\boldsymbol{\rho}$ using the image morphology operators "erode" and "dilate", respectively. In practice we may choose to optimize for just the eroded and the original topology or just for the original and the dilated topology. In the following, however, we formulate the problem for the use of all three density distributions simultaneously. The goal of the optimization problem is to maximize the objective function for the worst case of the three density distributions, i.e. a min-max formulation. In this way, we make sure that the optimized structure performs well both for a correctly etched structure but also for the over- and the under-etched structure.

The optimization problem can be formally written as

$$
\left.
\begin{aligned}
\min_{\boldsymbol{\rho}} &: \max\left(f(\boldsymbol{\rho}^e(\boldsymbol{\rho})), f(\boldsymbol{\rho}), f(\boldsymbol{\rho}^d(\boldsymbol{\rho}))\right) \\
s.t. &: \mathbf{K}(\boldsymbol{\rho}^e(\boldsymbol{\rho}))\mathbf{U}^e = \mathbf{F}, \\
&: \mathbf{K}(\boldsymbol{\rho})\mathbf{U} = \mathbf{F}, \\
&: \mathbf{K}(\boldsymbol{\rho}^d(\boldsymbol{\rho}))\mathbf{U}^d = \mathbf{F}, \\
&: g = V(\boldsymbol{\rho})/V^* - 1 \leq 0 \\
&: \mathbf{0} \leq \boldsymbol{\rho} \leq \mathbf{1}
\end{aligned}
\right\},
\tag{1}
$$

where $f(\cdot)$ is the objective function, $\mathbf{K}(\cdot)$ is the stiffness matrix, $\mathbf{U}$ is the displacement vector, $\mathbf{F}$ is the (here assumed design independent) load vector and V^* is the maximum bound on material volume. The Young's modulus of the material in each element is modelled by the usual SIMP interpolation law $E(\rho_e) = E_{min} + \rho_e^p(E_1 - E_{min})$, where E_{min} and E_1 are the Young's moduli of void (non-zero to avoid ill-conditioning) and solid material, respectively, and p is the penalization power that ensures solid/void (black and white) solutions to the optimization problem. Note that in spite of the three density vectors $\boldsymbol{\rho}$, $\boldsymbol{\rho}^e$ and $\boldsymbol{\rho}^d$, we only operate with the usual (one) design variable vector $\boldsymbol{\rho}$; the two others are explicit functions of $\boldsymbol{\rho}$. The problem formulation (1) holds for any topology optimization problem that is modelled by linear finite element analysis and one simple volume constraint but may easily be extended to dynamic, nonlinear or coupled problems and extra constraints may be added if needed.

As seen, the robust formulation of the optimization problem (1) requires three solutions of the underlying finite element problem, one for the original structure, one for the eroded structure and one for the dilated structure. In future studies we will investigate whether the re-analysis techniques suggested by Kirsch and co-workers [31–33] may be applied to speed up the computations.

3 Image morphology-based filter operators

In image analysis, morphology operators are used to quantify holes or objects, restore noisy pictures and perform automatic inspection of image data [34]. The basic morphology operators are "erode" and "dilate". An original binary topology image is shown in Fig. 2a. In image processing one defines a so-called "structuring element", here called the element "neighborhood" which will be defined below. Performing the morphology operation called erode, verbally corresponds to translating the center of the neighborhood over each element in the design domain. If any of the pixels covered by the neighborhood is void, then the center pixel is made void. Oppositely, the dilate operation sets the center pixel to solid if any pixel covered by the neighborhood is solid. The results of the two operations are seen in Fig. 2b and c. The dilate operator fills any hole that is smaller than the neighborhood (Fig. 2b). Oppositely, the erode operator removes any feature in the original image which is smaller than the neighborhood (Fig. 2c).

To make the discrete natured morphology operators applicable to gradient-based optimization they need to be redefined as continuous and differentiable functions. There are different ways to do this as discussed in ref. [16]. Here we use a smoothed Heaviside step function approach as suggested in ref. [15] and extended in [16]. In the following, we briefly discuss the definition of the neighborhood (structuring element), the original density filter and the implementation of the morphology operators "dilate" and "erode". For an extensive discussion of other morphology operators applicable to feature size control in topology optimization the reader is referred to the author's recent paper [16].

Structuring element

The neighborhood (structuring element) of element e, here named N_e, is specified as the elements that have centers within a given filter radius R of the center of element e, i.e.

$$
N_e = \{i \mid ||\mathbf{x}_i - \mathbf{x}_e|| \leq R\},
\tag{2}
$$

where $\mathbf{x}_i$ is the spatial (center) coordinate of element i and $||\cdot||$ denotes distance.

Density filtering

Traditional density filtering introduced in refs. [13,14] provides the basis for the morphology filters. The filtered density measure is

$$
\tilde{\rho}_e = \frac{\sum\limits_{i \in N_e} w(\mathbf{x}_i) v_i \rho_i}{\sum\limits_{i \in N_e} w(\mathbf{x}_i) v_i},
\tag{3}
$$

where v_i denotes the volume of element i and the weighting function $w(\mathbf{x}_i)$ is given by the linearly decaying (cone-shape) function

$$
w(\mathbf{x}_i) = R - ||\mathbf{x}_i - \mathbf{x}_e||.
\tag{4}
$$

Dilate

In its discrete form the dilation operator is a max-operator, i.e. the physical density of element e takes the maximum of the densities in the neighborhood N_e. The max-formulation is not suitable for gradient-based optimization and hence it must be converted to a continuous form.

A possible way to do this, as suggested for other reasons in ref. [15], is to modify the original density filter (3) with a Heaviside step-function such that if $\tilde{\rho}_e > 0$ then the physical element density will become one and only if the filtered density $\tilde{\rho}_e = 0$ will the physical density be zero. The Heaviside function is approximated as a smooth function governed by the continuation parameter β, thus the dilated density of element e, ρ_e^d, becomes

$$\rho_e^d = 1 - e^{-\beta \tilde{\rho}_e} + \tilde{\rho}_e e^{-\beta}. \tag{5}$$

For β equal to zero, this filter corresponds exactly to the original density filter (3). For β approaching infinity, the modification efficiently behaves as a max-operator, i.e. the density value of the center pixel is set equal to one if any one of the pixels within the neighborhood is larger than zero. For the examples presented in this paper we have found that a maximum value of $\beta = 16$ is sufficient for getting near solid-void solutions. In order to prevent numerical problems the value of β is increased from 1 to 16 gradually during the optimization process as will be discussed later.

Erode

In ref. [16] it was suggested to invert the Heaviside filter in order to use it as an "erode" operator. The modified Heaviside step function is again converted to a smooth function governed by the parameter β

$$\rho_e^e = e^{-\beta(1-\tilde{\rho}_e)} - (1 - \tilde{\rho}_e)e^{-\beta}. \tag{6}$$

Again, for β equal to zero, this filter corresponds to (3) and for β approaching infinity, the modification efficiently behaves as a min-operator.

4 Sensitivity analysis and numerical implementation

The sensitivities of the objective function with respect to the design variables must be found for each of the three material distributions. For the original density distribution $\boldsymbol{\rho}$ we find the sensitivities $\partial f(\boldsymbol{\rho})/\partial \rho_e$ in the usual way (defined for the three example problems in the Appendix). For the the dilated density distribution we may write the objective function as $\tilde{f} = f(\boldsymbol{\rho}^d(\boldsymbol{\rho}))$ and hence we use the chain rule to get

$$\frac{\partial \tilde{f}}{\partial \rho_e} = \sum_{i \in N_e} \frac{\partial \tilde{f}}{\partial \rho_i^d} \frac{\partial \rho_i^d}{\partial \tilde{\rho}_i} \frac{\partial \tilde{\rho}_i}{\partial \rho_e}, \tag{7}$$

and likewise with superscript d substituted with e for the eroded density distribution. Here, the sensitivity of the fil-

tered density $\tilde{\rho}_i$ with respect to a change in design variable ρ_e is found as

$$\frac{\partial \tilde{\rho}_i}{\partial \rho_e} = \frac{w(\mathbf{x}_e)v_e}{\sum_{j \in N_i} w(\mathbf{x}_j)v_j}. \tag{8}$$

For the dilate operator (5), the derivative of the dilated density with respect to the filtered density becomes

$$\frac{\partial \rho_i^d}{\partial \tilde{\rho}_i} = \beta e^{-\beta \tilde{\rho}_e} + e^{-\beta} \tag{9}$$

and for the erode operator (6) we get

$$\frac{\partial \rho_i^e}{\partial \tilde{\rho}_i} = \beta e^{-\beta(1-\tilde{\rho}_e)} + e^{-\beta}. \tag{10}$$

The sensitivities of the objective functions with respect to the dilated and eroded densities $\partial f(\boldsymbol{\rho}^d)/\partial \rho_i^d$ and $\partial f(\boldsymbol{\rho}^e)/\partial \rho_i^e$ are simply found using the sensitivity expressions in the appendix with $\boldsymbol{\rho}$ substituted by $\boldsymbol{\rho}^d$ and $\boldsymbol{\rho}^e$, respectively.

A main computational burden of the filtering schemes is to find the neighbors to each element. This is especially true in the case of irregular meshes. Therefore, ref. [16] suggests to compute a "neighborhood" matrix $\mathbf{N}$ that contains rows with neighbors to each element in the structure once and for all before the optimization begins. Following this idea, a very simplified flow chart in pseudo code may look like

1. Build neighborhood matrix $\mathbf{N}$
2. Initialize design variable vector $\boldsymbol{\rho}$, iter=0, change=1 and $\beta = 1$
3. while change>0.01 and iter $\leq$ 1000
4.   iter = iter + 1
5.   Compute filtered densities $\tilde{\boldsymbol{\rho}}$ using (3)
6.   Compute dilated densities $\boldsymbol{\rho}^d$ using (5) and eroded densities $\boldsymbol{\rho}^e$ using (6)
7.   Solve 3 FE problem based on $\boldsymbol{\rho}$, $\boldsymbol{\rho}^d$ and $\boldsymbol{\rho}^e$
8.   Calculate sensitivities

$$\frac{\partial f(\boldsymbol{\rho})}{\partial \tilde{\rho}_e}, \frac{\partial f(\boldsymbol{\rho}^d)}{\partial \tilde{\rho}_e} \text{ and } \frac{\partial f(\boldsymbol{\rho}^e)}{\partial \tilde{\rho}_e} \tag{11}$$

9.   Compute final sensitivities from (7) using (8-10)
10.   Update design variables $\boldsymbol{\rho}_{new}$ using MMA
11.   Calculate change = $||\rho_{new} - \rho||_\infty$
12.   if { 'mod(iter,50)=1' or 'change<0.01' and '$\beta \leq \beta_{max}$' } then
          $\beta = 2\beta$
          change = 0.5
13. end

Here, $\beta_{max} = 16$ is the maximum value of β for the continuation process.

The final algorithm is implemented in Matlab and uses the Method of Moving Asymptotes (MMA) [35]. The non-differentiability of the min-max formulation is avoided by solving it using a standard bound formulation which is a standard option in MMA.

	$N_x \cdot N_y$	R	f	V/V^*	Eroded ρ^e	Original ρ	Dilated ρ^d
a	$60 \cdot 20$	1.4/60	255.4 193.0 168.2	0.37 0.50 0.62			
b	$120 \cdot 40$	1.4/60	266.9 193.5 169.4	0.36 0.50 0.63			
c	$240 \cdot 80$	1.4/60	274.2 196.2 172.2	0.36 0.50 0.64			
d	$120 \cdot 40$	1.4/120	226.0 190.7 177.3	0.42 0.50 0.58			
e	$240 \cdot 80$	1.4/120	235.0 192.8 176.0	0.40 0.50 0.61			
f	$240 \cdot 80$	1.4/240	208.3 190.7 181.0	0.45 0.50 0.58			

Fig. 3 Robust topology optimization of the MBB beam. N_x and N_y denote number of elements in the horizontal and vertical directions, respectively and the columns named f and g with three numbers in each cell denote the compliances and volume fractions for the three topologies, respectively. a-c) filter size $R = 1.4/60$, d-e) filter size $R = 1.4/120$ and f) filter size $R = 1.4/240$.

5 Examples

5.1 MBB beam

As the first test case we use the well-known minimum compliance MBB beam example. The exact formulation of the design problem is given in the appendix and the volume fraction is 50%. The problem is solved for a number of different discretizations ($N_x \times N_y$) and filter sizes R. The optimized (half-beam) topologies are show in Fig. 3. The figure shows both the eroded, original and dilated density distribution for each case. From studying the figures, it is clear that the robust design formulation also ensures mesh-independent designs as expected since the morphology filters have the same properties as the traditional density filters [13,14]. Figs. 3a-c) have the same filter size but increasing mesh refinement and they all have the same topology. Likewise, for half the filter size Figs. 3d-e) also show convergence to a more complicated topology with mesh refinement. Finally, Figs. 3f) shows the result for fine resolution and small filter size. Here it is seen that checkerboards are still prevented although small structural details are not.

Due to the monotonous dependence on material density for compliance objective functions, it is obvious that the eroded topology always will have the highest compliance. This means that in practice, the min-max formulation here simply corresponds to minimizing the compliance of the eroded topology – the original and dilated topologies do not influence on the optimization process. This means, that apart from producing nice mesh-independent and discrete optimal topologies, the advantages of the robust design formulation do not really appear for simple compliance minimization problems.

5.2 Compliant force inverter

As another and more challenging test example for evaluation of the robust design formulation we consider the much-used force inverter example [3]. Again, details of the optimization problems are described in the Appendix. First, we optimize the inverter using the conventional sensitivity filtering technique [3] (Fig. 4a), the density filtering technique [13,14] (Fig. 4b) and the morphology operator "close" [16] (Fig. 4c), for the discretization $N_x \times N_y = 100 \times 50$ and filter size $R = 1.4/50$. Studying the results it is clear that all three topologies suffer from the localized hinge problem. The inverter optimized using the sensitivity filter (Fig. 4a) has somewhat blurred one-node-connected hinges, the inverter optimized using the density filter (Fig. 4b) has thin intermediate-density localized hinges and the inverter optimized using the close filter (Fig. 4c) has discrete one-node-connected hinges. All three mechanisms would clearly become disconnected if over-etched during manufacturing. The localized hinge problem is further illustrated in Fig. 5a. This figure shows the (exaggerated) deformation pattern of the inverter topology optimized using the sensitivity filter from Fig. 4a. It is seen that the right-most beam is unbent meaning that all deformation is happening in the hinge regions as opposed to the S-shaped, distributed compliant deformations in the topologies shown in Figs. 5b-c (more details later). Localized deformations will cause large stress concentrations and high likelihood of failure.
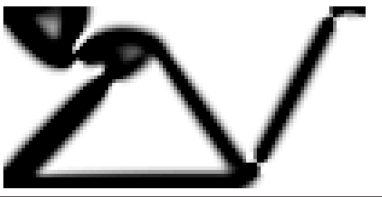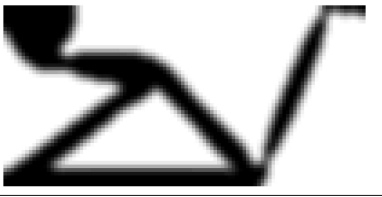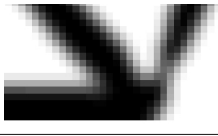
	$N_x \cdot N_y$	R	f	V/V^*	ρ Sensitivity filter	closeup of hinge region
a	$100 \cdot 50$	1.4/50	-2.25	0.30		
	$N_x \cdot N_y$	R	f	V/V^*	ρ Density filter	
b	$100 \cdot 50$	1.4/50	-2.13	0.30		
	$N_x \cdot N_y$	R	f	V/V^*	ρ Close filter	
c	$100 \cdot 50$	1.4/50	-2.55	0.30		

Fig. 4 Topology optimized compliant inverters using a) standard sensitivity filter, b) standard density filter and c) close filter.

To remedy above shortcoming, we solve the same topology optimization problem using the robust formulation with filter size $R = 1.4/100$, where we now the mechanism for the worst case of the eroded, original and dilated density distributions. The resulting topology (including the eroded and dilated density distributions) is shown in Fig. 6. The resulting eroded topology looks nice and is free from localized hinges, however, the original density distribution has some strange checkerboard-like grey regions and the dilated topology is seen to be extremely thick with a very high volume fraction. The problem is that the optimizer has taken advantage of a flaw in the problem formulation. As seen from the values of the objective function $f(\boldsymbol{\rho}^e) = -2.00$, $f(\boldsymbol{\rho}) = -2.19$ and $f(\boldsymbol{\rho}^d) = -2.00$, only the eroded and dilated density distributions are active in the min-max problem. The displacement of the original density distribution is smaller (more negative) than the two others and hence there is freedom to place superfluous material in the design domain which can aid either the eroded or dilated density cases in becoming better. In the present case, the checkerboard-like regions in the original density distribution cause extra stiff material in the dilated topology but do not disturb the eroded structure.

Different ideas can be envisioned to avoid this ill-conditioning of the optimization problem. One possibility could be to impose a volume constraint also on the dilated topology. However, the value of this constraint is difficult to choose since it is dependent on problem definition, the value of the original volume constraint and the filter size R. Another alternative could be to minimize the sum of the three objective functions instead of using the min-max formulation. In this way the algorithm also emphasizes the response for the original density distribution. As seen in Fig. 7, this works

fairly well, however, now the eroded and original topologies are optimized on the cost of a fairly low-performing dilated topology. Hence, this formulation is not very good either. Instead, we propose to formulate the problem in terms of two density distributions instead of three, i.e. we only optimize for the worst case of the eroded and the original density distributions. In this way we avoid the problem with the intermediate (original) density distribution being on a "free ride" between the eroded and dilated density distributions. In principle, one could also optimize for the original and dilated density distributions (with the volume constraint on the dilated density distribution) and get similar results. However, an advantage of using the eroded and original distributions is that the original density distribution is independent on the continuation parameter β and hence the erode/original scheme is expected to be more stable than the original/dilate scheme.

Fig. 8 shows the result of the inverter problem optimized for the worst case of the eroded and original density distributions for various discretizations and mesh resolutions.

Apart from convergence with mesh-refinement, Fig. 8 shows that the topology optimized inverters based on the robust formulation are indeed robust to manufacturing uncertainties. The mechanisms are all seen to be equally good (have same values of the objective functions) for both the eroded and original density distributions. Objective function values of the dilated density distributions which were not part of the optimization are given in parentheses in the table. As would be expected, their performances are very bad compared to those which were included in the optimization (the eroded and original distributions). Following these observations it is interesting to note that the one-node connected

$N_x \cdot N_y$	R	f	V/V^*	Eroded $\boldsymbol{\rho}^e$	Original $\boldsymbol{\rho}$	Dilated $\boldsymbol{\rho}^d$
$100 \cdot 50$	1.4/100	-2.00 -2.19 -2.00	0.21 0.30 0.52			

Fig. 6 Topology optimized compliant inverter based on the robust design approach using the worst case of the eroded, original and dilated density distributions.
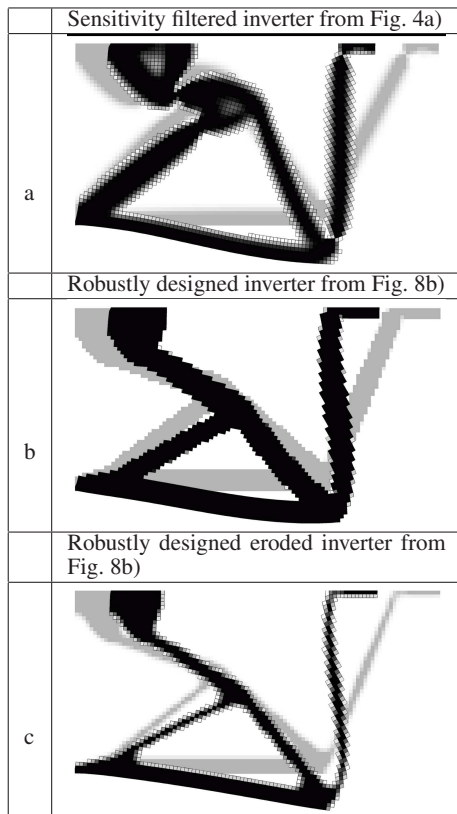
$N_x \cdot N_y$	R	f	V/V^*	Eroded $\boldsymbol{\rho}^e$	Original $\boldsymbol{\rho}$	Dilated $\boldsymbol{\rho}^d$
$100 \cdot 50$	1.4/50	-1.57 -1.79 -1.01	0.17 0.30 0.42			
$100 \cdot 50$	1.4/100	-2.09 -2.24 -1.78	0.24 0.30 0.36			

Fig. 7 Topology optimized compliant inverter based on the robust design approach using the *s*um of the objective functions for the eroded, original and dilated density distributions.

Sensitivity filtered inverter from Fig. 4a)

a

Robustly designed inverter from Fig. 8b)

b

Robustly designed eroded inverter from Fig. 8b)

c

Fig. 5 Deformations patterns of optimized topologies overlaid on dimmed pictures of the undeformed structures. a) The sensitivity filtered inverter from Fig. 4a, b) The robustly topology optimized inverter from Fig. 8b, and c) the eroded inverter from b).

hinge problem observed in Fig. 4 has been eliminated. For a finite filter size a one-node connected hinge in the original density distribution will become disconnected after the erosion process and hence the one-node connected hinges will never appear in an optimized structure. For a certain filter size (here $R > 1.4/100$) it also appears that the resulting mechanisms have distributed compliance, i.e. the deformation is distributed all over the mechanism and not only to defacto hinge regions. Based on tests, it is concluded that if the filter diameter corresponds to the thickness of the bars making up the compliant mechanism then the mechanism will become distributed compliant. For smaller filter sizes the mechanism will exhibit lumped compliance. A similar phenomenon can be observed in ref. [17]. This means that not only does the suggested approach provide etching tolerant designs, but it also resolves the longstanding problem of one-node connected hinges in topology optimization of compliant mechanisms and it partly solves the problem of localized hinges. These observations are further tested in the last example.

5.3 Determination of the "blue-print" design

With the suggested two-density field formulation only one question remains to be answered: which density distribution should be used as the input to the manufacturing process, i.e. what should the "blue-print" look like? Obviously, neither the eroded nor the original distributions will work well. The former will be very sensitive to over-etching and the original distribution will be very sensitive to under-etching. We suggest to use an eroded density distribution obtained from the original distribution but using a filter with half the radius
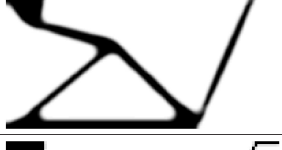
	$N_x \cdot N_y$	R	f	V/V^*	Eroded ρ^e	Original ρ	closeup of hinge region
a	$50 \cdot 25$	1.4/50	-1.68 -1.68 (-0.77)	0.18 0.30 (0.41)			
b	$100 \cdot 50$	1.4/50	-1.69 -1.69 (-0.73)	0.17 0.30 (0.42)			
c	$200 \cdot 100$	1.4/50	-1.67 -1.67 (-0.68)	0.16 0.30 (0.44)			
d	$100 \cdot 50$	1.4/100	-2.12 -2.12 (-1.51)	0.23 0.30 (0.38)			
e	$200 \cdot 100$	1.4/100	-2.11 -2.11 (-1.32)	0.23 0.30 (0.42)			
f	$200 \cdot 100$	1.4/200	-2.19 -2.19 (-1.69)	0.26 0.30 (0.41)			

Fig. 8 Topology optimized compliant inverters based on the robust design approach using the worst case of the eroded and original density distributions. The numbers in parentheses in the objective f and constraint function g columns indicate the displacement and the volume fraction of the associated dilated density distribution which here is not part of the optimization. a-c) filter size $R = 1.4/50$, d-e) filter size $R = 1.4/100$ and f) filter size $R = 1.4/200$.

of the filter used in the optimization. In this way, the "blue-print" density distribution obtained with the suggested two field approach will be robust towards both under- and over-etching. Using this approach, however, the blue-print design will have a volume fraction that is lower than the original volume constraint. Hence, to ensure the correct volume constraint, we may constrain the average of the original and the eroded volumes. The modified formulation of the original optimization problem (1) using the worst case of the eroded and original density distributions now becomes

$$
\left.
\begin{aligned}
\min_{\boldsymbol{\rho}} &: \max\left(f(\boldsymbol{\rho}^e(\boldsymbol{\rho})), f(\boldsymbol{\rho})\right) \\
s.t. &: \mathbf{K}(\boldsymbol{\rho}^e(\boldsymbol{\rho}))\mathbf{U}^e = \mathbf{F}, \\
&: \mathbf{K}(\boldsymbol{\rho})\mathbf{U} = \mathbf{F}, \\
&: g = \left(V(\boldsymbol{\rho}^e(\boldsymbol{\rho})) + V(\boldsymbol{\rho})\right)/2/V^* - 1 \le 0 \\
&: \mathbf{0} \le \boldsymbol{\rho} \le \mathbf{1}
\end{aligned}
\right\}.
\quad (12)
$$

After convergence the blue print design is found as the original density distribution $\boldsymbol{\rho}$ eroded with half the design filter radius, i.e. $\boldsymbol{\rho}^{blueprint} = \boldsymbol{\rho}^e_{R'=R/2}(\boldsymbol{\rho})$.

In order to ensure that this is a viable approach we test it on a final example.

5.4 Compliant gripper

The viability of the proposed procedure is tested on a final and topologically more complex example, i.e. the compliant gripper test case also originally suggested in [3]. Again, details of the optimization problem are described in the Appendix. First, we optimize the gripper using the conventional sensitivity filtering technique (Fig. 9a), the density filtering technique (Fig. 9b) and the close filtering technique (Fig. 9c) for the discretization $N_x \times N_y = 100 \times 50$ and filter size $R = 1.4/50$. Again, the optimized topologies are seen to suffer from the localized and one-node connected hinge problems.

In contrast, the grippers obtained using the robust formulation (Fig. 9d) and with finer resolution (Fig. 9e) are seen to be distributed compliant both for the eroded and original density distributions. Note that the volume constraint is now satisfied in an average sense according to the volume constraint in (12). The robust design is obtained on the cost of a reduction in the objective function ($f = -0.81$ compared to $f = -0.97$ obtained for the sensitivity filter).
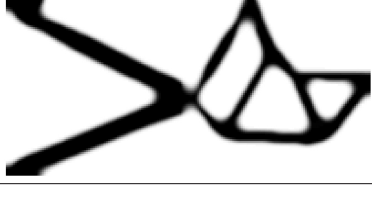
	$N_x \cdot N_y$	R	f	V/V^*	Eroded ρ^e	Original ρ
a	$100 \cdot 50$	1.4/50	-0.97	0.30	NA	
b	$100 \cdot 50$	1.4/50	-0.84	0.30	NA	
c	$100 \cdot 50$	1.4/50	-1.06	0.30	NA	
d	$100 \cdot 50$	1.4/50	-0.81 -0.81	0.22 0.38		
e	$200 \cdot 100$	1.4/50	-0.78 -0.78	0.21 0.39		

Fig. 9 Topology optimized compliant grippers. a) Conventional sensitivity filter, b) conventional density filter, c) close filter, d) robust formulation with erode and original density distributions and e) same as d) but with finer discretization.

To obtain the blue-print design we erode the original density distributions from Figures 9d and e using half the filter size, i.e. $R' = R/2 = 1.4/100$. To check the robustness of the blue-print designs we then calculate the performance of the blue-print design as well as this design eroded and dilated with half the filter size, respectively. The results of this study are shown in Figure 10. Panels a and c show the topologies of the optimization study (repeated from Figure 9) and panels b and d show the blue-print design (center) and the half-filter eroded and dilated designs (left and right, respectively). Ideally, the two latter should correspond to the original optimization results, however, due to the filters being of non-perfect round shape (the discretization of the round filter is quite bad for small filter sizes), there is a discrepancy between the performances. Nevertheless, there are only small differences in the performances which supports the viability of the approach in ensuring manufacturing tolerant designs. To ensure even better robustness one may during the optimization choose to work with a filter radius somewhat larger than the desired robustness tolerance.

6 Discussion and conclusions

The suggested robust topology optimization formulation has been proved to work well and to resolve the long-standing problem of one-node connected hinges in topology optimization of compliant mechanisms. Further, if the filter size is selected large enough the optimized topologies tend to be of the distributed compliance type. However, these features are accompanied by a number of disadvantages. First, one needs to solve the finite element problem at least twice for each optimization iteration – once for the original density distribution and once for the eroded density distribution. This problem may be overcome by the use of efficient reanalysis techniques as suggested in refs. [31–33]. Alternatively, the fully decoupled problems are easily solved in parallel. Second, the continuation approach necessary for implementing
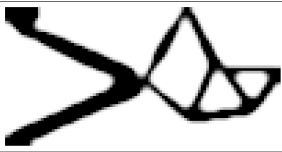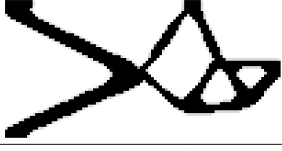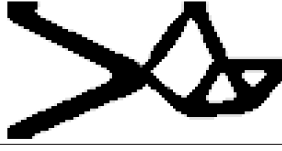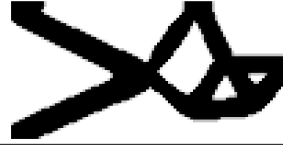
	R	f	V/V^*	Eroded ρ^e	Original ρ	Dilated ρ^d
a	1.4/50	-0.81 -0.81	0.22 0.38			NA
b	1.4/100	-0.86 -0.94 -0.75	0.23 0.31 0.39			
c	1.4/50	-0.78 -0.78	0.21 0.39			NA
d	1.4/100	-0.69 -0.89 -0.69	0.20 0.30 0.39			

Fig. 10 Obtaining the blue-print design. a) Optimized gripper obtained using the robust erode/original formulation (12). b) The original density distribution from a) is eroded with half the filter size (center) and then eroded (left) and dilated (right) density distributions are created with this structure as basis.

the morphology filter erode is rather delicate and needs careful tuning. Increasing the continuation parameter β too fast may cause failure of the algorithm and likewise the maximum value β_{max} should be chosen with care. A too small value causes blurred and not well-defined topologies and a too large value causes non-differentiability of the problem. Third, choosing the filter size R too large may cause failure of the algorithm since the eroded density distribution may get totally dissolved. The latter problem however, is of physical nature and tells the user that he has selected too small a volume fraction, a too large filter or that he has to improve his manufacturing process. Having mentioned all these problems, it should be noted that all the examples in this paper have been produced by one simple batch run. No tweaking of parameters have been performed in order to fine tune some of the examples.

The examples shown in this paper were performed for regular meshes with square finite elements. However, there are no problems in extending the idea to unstructured meshes.

Several possibilities for further studies may be envisioned. Instead of using the eroded and original density distributions, one could also work with the eroded and "closed" density distributions. In this way one can make sure that there are no small holes in the original density distribution and at the same time ensure robustness with respect to over-etching. Other combination of morphology-based filters could also be considered (see ref. [16] for a discussion of morphology filters in connection with topology optimization). A possibility could be anisotropic filter operators that could take unidirectional manufacturing uncertainties into account.

Finally, it may be interesting to look into other manufacturing problems like proximity effects in laser and e-beam processes [36] where the etch-rate may depend on distance between holes.

References

1. Borel, P.I., Harpøth, A., Frandsen, L.H., Kristensen, M., Jensen, J.S., Shi, P., Sigmund, O.: Topology optimization and fabrication of photonic crystal structures. Optics Express **12**(9), 1996–2001 (2004). Http: //www.opticsexpress.org/abstract.cfm?URI=OPEX-12-9-1996
2. Borel, P.I., Frandsen, L.H., Harpøth, A., Kristensen, M., Jensen, J.S., Sigmund, O.: Topology optimised broadband photonic crystal Y-splitter. Electronics Letters **41**(2), 69–71 (2005)
3. Sigmund, O.: On the design of compliant mechanisms using topology optimization. Mechanics of Structures and Machines **25**(4), 493–524 (1997)
4. Sigmund, O.: Design of multiphysics actuators using topology optimization - Part I: One-material structures. Computer Methods in Applied Mechanics and Engineering **190**(49-50), 6577–6604 (2001). DOI 10.1016/S0045-7825(01)00251-1
5. Yin, L., Ananthasuresh, G.: Design of distributed compliant mechanisms. Mechanics Based Design of Structures and Machines **31**(2), 151–179 (2003)
6. Díaz, A.R., Sigmund, O.: Checkerboard patterns in layout optimization. Structural Optimization **10**(1), 40–45 (1995)
7. Jog, C.S., Haber, R.B.: Stability of finite element models for distributed-parameter optimization and topology design. Com-

puter Methods in Applied Mechanics and Engineering **130**(3-4), 203–226 (1996)

8. Sigmund, O., Petersson, J.: Numerical instabilities in topology optimization: A survey on procedures dealing with checkerboards, mesh-dependencies and local minima. Structural Optimization **16**(1), 68–75 (1998)

9. Poulsen, T.A.: A new scheme for imposing a minimum length scale in topology optimization. Int. Journal Numerical Methods in Engineering **57**(6), 741–760 (2003)

10. Yoon, G.H., Kim, Y.Y., Bendsøe, M.P., Sigmund, O.: Hinge-free topology optimization with embedded translation-invariant differentiable wavelet shinkage. Structural and Multidisciplinary Optimization **27**(3), 139–150 (2004)

11. Rahmatalla, S., Swan, C.: Sparse monolithic compliant mechanisms using continuum structural topology optimization. International Journal for Numerical Methods in Engineering **62**(12), 1579–605 (2005)

12. Saxena, A.: Design of nonlinear springs for prescribed load-displacement functions. Journal of Mechanical Design **130**(8), 081,403 (2008)

13. Bruns, T.E., Tortorelli, D.A.: Topology optimization of non-linear elastic structures and compliant mechanisms. Computer Methods in Applied Mechanics and Engineering **190**(26-27), 3443–3459 (2001)

14. Bourdin, B.: Filters in topology optimization. International Journal for Numerical Methods in Engineering **50**(9), 2143–2158 (2001)

15. Guest, J., Prevost, J., Belytschko, T.: Achieving minimum length scale in topology optimization using nodal design variables and projection functions. International Journal for Numerical Methods in Engineering **61**(2), 238–254 (2004)

16. Sigmund, O.: Morphology-based black and white filters for topology optimization. Structural and Multidisciplinary Optimization **33**(4-5), 401–424 (2007)

17. Luo, J., Luo, Z., Chen, S., Tong, L., Wang, M.Y.: A new level set method for systematic design of hinge-free compliant mechanisms. Computer Methods in Applied Mechanics and Engineering **198**(2), 318–331 (2008)

18. Pedersen, C.B.W., Buhl, T., Sigmund, O.: Topology synthesis of large-displacement compliant mechanisms. International Journal of Numerical Methods in Engineering **50**(12), 2683–2705 (2001)

19. Ben-Tal, A., Nemirovski, A.: Robust truss topology design via semidefinite programming. SIAM Journal on Optimization **7**(4), 991–1016 (1997)

20. Chen, J., Cao, Y., Sun, H.: Topology optimization of truss structures with systematic reliability constraints under multiple loading cases. Acta Mechanica Solida Sinica **12**(2), 165–173 (1999)

21. Christiansen, S., Patriksson, M., Wynter, L.: Stochastic bilevel programming in structural optimization. Structural and Multidisciplinary Optimization **21**(5), 361–371 (2001)

22. Maute, K., Frangopol, D.: Reliability-based design of MEMS mechanisms by topology optimization. Computers and Structures **81**(8-11), 813–824 (2003)

23. Kharmanda, G., Olhoff, N., Mohamed, A., Lemaire, M.: Reliability-based topology optimization. Structural and Multidisciplinary Optimization **26**(5), 295–307 (2004)

24. Kang, J., Kim, C., Wang, S.: Reliability-based topology optimization for electromagnetic systems. COMPEL: The International Journal for Computation and Mathematics in Electrical and Electronic Engineering **23**(3), 715–723 (2004)

25. Jung, H.S., Cho, S.: Reliability-based topology optimization of geometrically nonlinear structures with loading and material uncertainties. Finite Elements in Analysis and Design **41**(3), 311–331 (2004)

26. Mogami, K., Nishiwaki, S., Izui, K., Yoshimura, M., Kogiso, N.: Reliability-based structural optimization of frame structures for multiple failure criteria using topology optimization techniques. Structural and Multidisciplinary Optimization **32**(4), 299–311 (2006)

27. Kim, C., Wang, S., Hwang, I., Lee, J.: Application of reliability-based topology optimization for microelectromechanical systems. AIAA Journal **45**(12), 2926 (2007)

28. Seepersad, C., Allen, J., McDowell, D., Mistree, F.: Robust design of cellular materials with topological and dimensional imperfections. Journal of Mechanical Design, Transactions of the ASME **128**(6), 1285–1297 (2006)

29. Guest, J., Igusa, T.: Structural optimization under uncertain loads and nodal locations. Computer Methods in Applied Mechanics and Engineering (2008). DOI doi:10.1016/j.cma.2008.04.009. In press

30. Sigmund, O.: A 99 line topology optimization code written in MATLAB. Structural and Multidisciplinary Optimization **21**, 120–127 (2001). DOI 10.1007/s001580050176. MATLAB code available online at: www.topopt.dtu.dk

31. Kirsch, U.: Reduced basis approximations of structural displacements for optimal design. AIAA Journal **29**(10), 1751–1758 (1991)

32. Kirsch, U.: Reanalysis of Structures, *Solid Mechanics and its applications*, vol. 151. Springer (2008)

33. Amir, O., Bendsøe, M.P., Sigmund, O.: Approximate reanalysis in topology optimization. Internal journal for numerical methods in engineering (2009). DOI 10.1002/nme.2536. Published online December 23rd 2008

34. Pratt, W.K.: Digital Image Processing. John Wiley and Sons, New York (1991)

35. Svanberg, K.: The Method of Moving Asymptotes - A new method for structural optimization. International Journal for Numerical Methods in Engineering **24**, 359–373 (1987)

36. Suzuki, K., Smith, B.W. (eds.): Microlithography: Science and Technology. CRC Press (2007)

37. Sigmund, O.: Mechanics for a New Millenium, chap. Optimum deisgn of microelectromechanical systems, pp. 505–520. Kluwer Academic Publishers, Netherlands (2001)

38. Bendsøe, M.P., Sigmund, O.: Topology Optimization - Theory, Methods and Applications. Springer Verlag, Berlin Heidelberg, XIV+370 pp. (2003)

A Definition of test problems

The three test cases are based on the standard "density based approach to topology optimization", i.e. the design variables $\boldsymbol{\rho}$ represent piece-wise constant element densities. We consider linear isotropic materials and the Young's modulus of an element is a function of the element design variable ρ_e given by the modified SIMP (Simplified Isotropic Material with Penalization) interpolation scheme

$$E_e = E(\rho_e) = E_{min} + \rho_e^p (E_0 - E_{min}), \quad \rho_e \in [0,1], \qquad (13)$$

where p is the penalization power, E_{min} is the stiffness of soft (void) material (non-zero in order to avoid singularity of the stiffness matrix) and E_0 is the Young's modulus of solid material. The test structures are discretized by 4-node bi-linear finite elements. Otherwise, the implementation is done in MATLAB as described in [30] with the MATLAB implementation of the Method of Moving Asymptotes [35] substituting the Optimality Criteria approach as the optimizer.

In the following we define the three problem specific formulations. Remark that the problems are defined in terms of the original density vector $\boldsymbol{\rho}$, however, the needed values for the dilated and eroded density distributions are simply found by substituting $\boldsymbol{\rho}$ with $\boldsymbol{\rho}^d$ and $\boldsymbol{\rho}^e$, respectively.

A.1 The MBB-beam

The minimum compliance objective function for the MBB-beam example may be written as

$$f(\boldsymbol{\rho}) = \mathbf{U}^T \mathbf{K} \mathbf{U} = \sum_e \mathbf{u}_e^T \mathbf{k}_e \mathbf{u}_e \tag{14}$$

and the volume constraint may be written as

$$g = V(\boldsymbol{\rho})/V^* - 1 = \sum_e v_e \rho_e / V^* - 1 \le 0 \tag{15}$$

where $\mathbf{K}$, $\mathbf{U}$ and $\mathbf{F}$ are the global stiffness matrix, displacement vector and force vector, respectively, lower case symbols indicate element wise quantities, $\mathbf{k}_e = \mathbf{k}(\rho_e) = E(\rho_e)\mathbf{k}_e^0$, is the element stiffness matrix, $\mathbf{k}_e^0$ is the element stiffness matrix for unit Young's modulus, V^* is the material resource constraint and v_e is the volume of element e. The sensitivity expressions are simply found as

$$\frac{\partial f}{\partial \rho_e} = -\mathbf{u}_e^T \frac{\partial \mathbf{k}_e}{\partial \rho_e} \mathbf{u}_e,$$
$$\frac{\partial \mathbf{k}_e}{\partial \rho_e} = p\,(E_0 - E_{min})\rho_e^{p-1}\mathbf{k}_e^0, \tag{16}$$
$$\frac{\partial g}{\partial \rho_e} = v_e/V^*.$$

The design domain and its dimensions are shown in Fig. 11a Due to symmetry we model only half the design domain which is discretized with N_x by N_y bi-linear quadrilaterals. The Young's modulus of solid material is $E_0 = 1$, the minimum stiffness is $E_{min} = 10^{-9}$, the Poisson's ratio is $\nu = 0.3$ and the penalization factor is $p = 3$.

A.2 The compliant force inverter

In compliant mechanism design, a typical design goal is to transfer work from an input actuator to an output spring, cf. [37,38]. For the present case, we consider the force inverter that previously has been used as a benchmark. The displacement objective function for the inverter optimization problem may be written as

$$f(\boldsymbol{\rho}) = \mathbf{L}^T \mathbf{U} \tag{17}$$

where $\mathbf{L}$ is a unit length vector with zeros at all degrees of freedom except at the output point where it is one. The sensitivity is simply found as

$$\frac{\partial f}{\partial \rho_e} = \lambda_e^T \frac{\partial \mathbf{k}_e}{\partial \rho_e} \mathbf{u}_e, \tag{18}$$

where λ is the global adjoint vector found by the solution of the adjoint problem $\mathbf{K}\lambda = -\mathbf{L}$ and λ_e is the part of the adjoint vector associated with element e. The design domain and its dimensions are shown in Fig. 11b. For faster computations we consider only half the structure due to symmetry. The design domain is discretized with N_x by N_y bi-linear quadrilaterals, the input force is $F_{in} = 1$ and the input and output spring stiffnesses are $k_{in} = 1$ and $k_{out} = 0.001$, respectively. Otherwise, the parameters are the same as for the
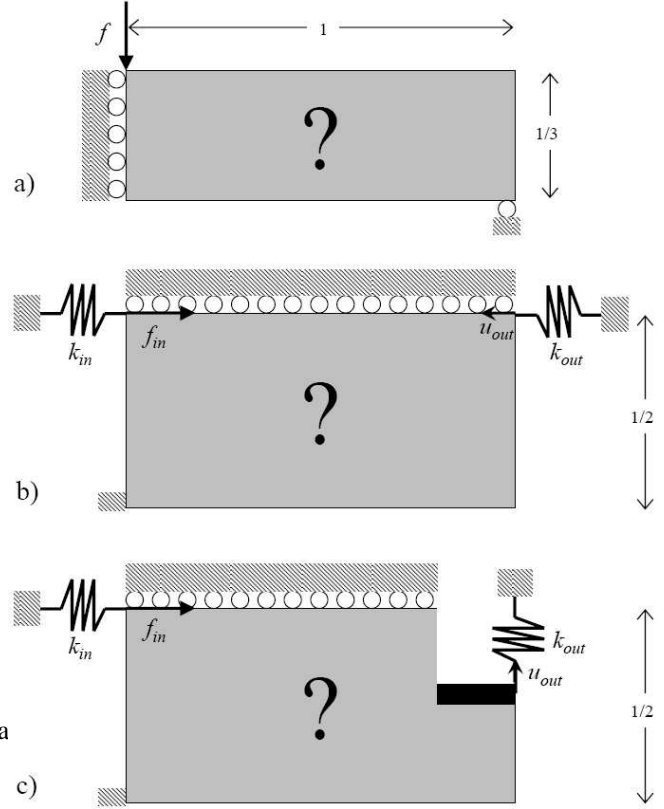

Fig. 11 Design domains and boundary conditions for the three test problems. a) The MBB-beam, b) the compliant force inverter and c) the compliant gripper.

MBB example. Remark that the input and output spring stiffnesses are chosen such that the resulting mechanism without filtering exhibits so-called one-node-connected hinges. For higher stiffness of the output spring, the hinge-like connection becomes more solid (distributed compliant) on the cost of smaller output displacement [3]. In order to demonstrate the ability of the robust design formulation to produce distributed compliant hinges as opposed to the conventional one-node connected hinges, we here select a small value of the output spring stiffness.

In general, the inverter problem is hard to solve. The most direct solution when minimizing the output displacement (which is clearly a local minimum) is to make the output displacement zero by disconnecting it from the rest of the structure. This local minimum is a large attractor and in many cases optimization algorithms may get stuck here and do not manage to produce a negative (inverting) displacement mechanism. The proposed min-max formulation seems to be especially vulnerable to this problem. In order to circumvent it, we minimize the sum of the objective functions for the first 10 iterations and thereafter switch to the proposed min-max strategy. For all the test cases this idea has prevented the algorithm in getting stuck in the local minimum.

A.3 The compliant gripper

Apart from the geometry that involves a non-design domain (indicated with black in Fig. 11c), except for the output spring stiffness that has been changed to $k_{out} = 0.005$ all the values for the gripper example corresponds to those of the force inverter example.